Journal of The Electrochemical Society, **158** (12) A1379-A1382 (2011)
0013-4651/2011/158(12)/A1379/4/$28.00 © The Electrochemical Society

$CoMn_2O_4$ Spinel Nanoparticles Grown on Graphene as Bifunctional Catalyst for Lithium-Air Batteries

Long Wang,[a] Xin Zhao,[a] Yuhao Lu,[a] Maowen Xu,[a] Dawei Zhang,[c] Rodney S. Ruoff,[a] Keith J. Stevenson,[b] and John B. Goodenough[a,z]

[a]*Materials Science and Engineering Program and Texas Materials Institute and* [b]*Department of Chemical Engineering and Department of Chemistry and Biochemistry, The University of Texas at Austin, Austin, Texas 78712, USA*
[c]*Hefei University of Technology, School of Chemistry and Engineering, Hefei 230009, People's Republic of China*

Positive electrodes for the oxygen reduction reaction (ORR) and the oxygen-evolution reaction (OER) play a critical role in fuel cells and metal-air batteries. Tetragonal $CoMn_2O_4$ spinel nanoparticles have been grown on the surface of graphene sheets (CMOG) via a two-step synthesis. The ORR/OER catalytic characteristics of CMOG were studied with a rotating-disk electrode. Also a lithium-air primary cell having a non-aqueous electrolyte and a rechargeable lithium-air cell with a Li-ion solid electrolyte separating a non-aqueous anode electrolyte from an alkaline aqueous cathode electrolyte were assembled with a CMOG cathode and tested. The results indicate that a CMOG cathode can provide a catalytic platform of considerable activity for the ORR in both electrolytes and also for the OER in the aqueous electrolyte.
 [DOI: 10.1149/2.068112jes]

Manuscript submitted July 20, 2011; revised manuscript received September 12, 2011. Published November 4, 2011.

A secondary Li-air battery would have a theoretical energy density of 5200 Wh kg^{-1} based on full utilization of a lithium anode. Conventional Li-ion batteries containing an insertion-compound cathode have energy densities that rarely exceed 1000 Wh kg^{-1}. A Li-air battery has a catalyst-loaded carbon cathode with access to air.[1–3] The catalyst should be inexpensive and highly active for the oxygen reduction reaction (ORR) if a primary battery, but also for the oxygen-evolution reaction (OER) if a secondary battery. The group of Yang Shao-horn has developed Pt-Au nanoparticles as bifunctional catalyst that dramatically reduce the voltage gap between the ORR and OER to less than 0.8 V at 50 mA g^{-1}.[4] Thapa[5]also combined α-MnO_2 with Pd to decrease the gap in a Li-air battery. However, these strategies use expensive noble metals as catalyst, and their cost may prevent their use in large-scale applications.

Oxospinels containing Ni, Co and/or Mn have been widely reported[6–9] to be active catalysts for the ORR and OER in Zn-air batteries[10,11] with Co and Mn having, respectively, favorable activity for the OER and ORR. However, preparation of those spinels by traditional high-temperature sintering gives particles of large size and therefore small surface area. Recently, Cheng et al.[12] reported a room temperature synthesis of $CoMn_2O_4$ nanoparticles having good ORR and OER catalytic activities. Since $CoMn_2O_4$ spinel is a semiconductor and good catalytic activity requires fast electron transport, the $CoMn_2O_4$ spinel nanoparticles require attachment to a conducting surface, preferably a carbon surface.

Among the myriad carbon materials, graphene sheets offer a theoretical specific surface area as high as 2630 m^2 g^{-1} as well as high mechanical strength and electronic conductivity. Therefore, graphene/transition-metal-oxide compositions have been investigated as energy storage materials,[13,14] and a MoS_2/graphene composite prepared solvothermally has been reported to be a hydrogen evolution catalyst.[15] Pt particles have also been grown on graphene to evaluate the 2D ORR catalyst.[16,17] Graphene has been claimed[18] to exhibit ORR activity as a result of abundant defects; but the published data indicate the activity of graphene alone is insufficient.[19] Herein, we report on the ORR/OER bifunctional catalytic activity of $CoMn_2O_4$ nanoparticles grown on the surface of graphene sheets (CMOG). The bifunctional catalytic activity has been investigated with a rotating-disk electrode and in Li-air batteries assembled with non-aqueous and aqueous electrolytes in contact with a CMOG cathode exposed to oxygen.

Experimental

Graphene oxide sheets were prepared via a modified Hummer's method.[20–22] $CoMn_2O_4$-graphene composite (CMOG) was prepared by a two-step process: 40 mg graphene oxide sheets were dispersed in 150 mL dimethylformamide in a 500 mL flask and sonicated for 30 min. The well-dispersed suspension was kept at 80°C for 1 h with vigorous stirring. Cobalt acetate ($Co(CH_3CH_2COO)_2{\cdot}4H_2O$) and manganese acetate ($Mn(CH_3CH_2COO)_2{\cdot}4H_2O$) in a 1:2 molar ratio was dissolved into 20 mL deionized water (metal-ion concentration 0.2 M) and slowly added drop wise into the graphene oxide suspension. A black precipitate was re-dispersed in 120 mL deionized water and transferred into three 40 mL Teflon autoclaves. Hydrothermal treatment was conducted at 180°C for 10 h to obtain the final product CMOG.

Powder x-ray diffraction (XRD) data were collected in the 2θ range 10 to 90° with 0.02° step size and 12 s dwell time with a Philips X'pert diffractometer and Cu K_α radiation (λ = 1.54056 Å). The morphology and nanostructure of the CMOG was investigated with a transmission electron microscope (TEM, JEOL 2010F, 200 kV) and a holey carbon film on copper grid as a substrate. An energy dispersive x-ray spectroscopy (EDS) measurement has been conducted with an Oxford Inca spectrometer to determine the chemical composition of the CMOG.

Linear scanning voltammogram data were collected with an Auto Lab electrochemical workstation. 1 mg graphene oxide or CMOG or commercial Pt catalyst (20 wt % Pt on Vulcan XC 72, Premetek) powder and 1 mg XC-72 carbon were dispersed in a mixture of 250 μL deionized water and 50 μL Nafion to prepare a homogeneous ink;; a drop of 5 μL ink was put onto a 0.2 cm^2 glassy-carbon disk electrode and dried at room temperature. Voltammograms were measured in 0.1 M KOH solution saturated with oxygen. A Hg/Hg_2SO_4 electrode was used as the reference electrode. The voltage window was 0 to −1.0 V and 0 to 0.5 V for the ORR and the OER, respectively.

The performance of the CMOG cathode in a non-aqueous and in an alkaline aqueous electrolyte was compared with two test cells having the configuration described elsewhere.[23] In each cell the air electrode consisted of CMOG, acetylene black (AB) and polytetrafluoroethene (weight ratio 30:50:20) in an oxygen-saturated electrolyte (O_2 flow of 2 mL min^{-1}). The loading density of the positive electrode used in this study is about 2 mg cm^{-2}. In one test cell, the non-aqueous 1:1 v/v ethylene carbonate (EC) : dimethyl carbonate (DMC) electrolyte containing 1 M $LiPF_6$ was used with a glass-fiber separator; in the other, the non-aqueous electrolyte at the anode side was separated from a 1 M LiOH aqueous electrolyte at the cathode side by a 160-μm thick Li-ion solid electrolyte $Li_{1+x+y}Al_xTi_{2-x}Si_yP_{3-y}O_{12}$ from

[z] E-mail: jgoodenough@mail.utexas.edu

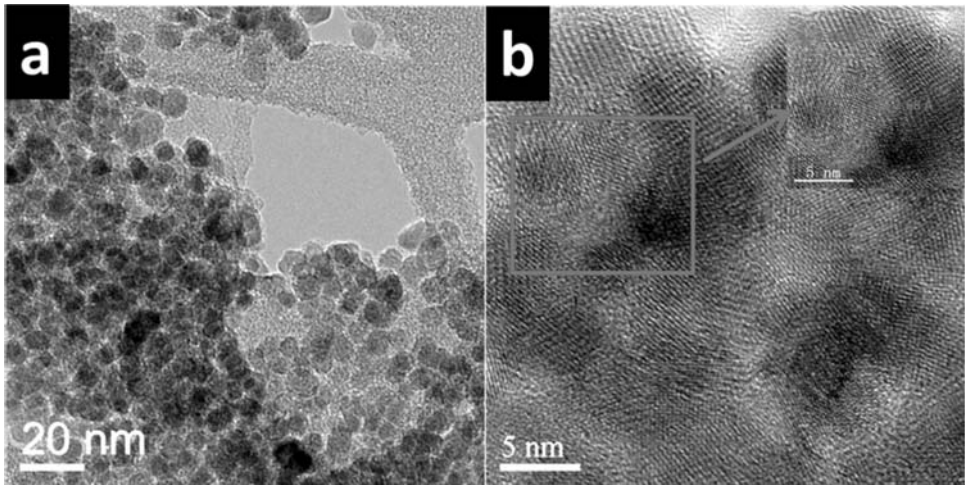

Figure 1. (a) TEM image and (b) HRTEM of the CMOG.

OHARO Inc., Japan. The test cell with non-aqueous electrolyte was cycled between 2.0 and 4.5 V versus lithium and the other one with a hybrid electrolyte was cycled between 2.5 and 4.0 V.

Results and Discussion

The TEM image (Fig. 1a) clearly shows the small particles have a narrow size distribution around 10 nm, and no obvious agglomeration can be seen. No graphene-free nanopartilces were observed during the TEM examination, indicating there is a good attachment between the graphene surface and the nanoparticles, which is similar to an early report.[14] Since every nanoparticle is separately fixed on the surface of the graphene sheets, they do not grow further during hydrothermal treatment. The HRTEM image of the CMOG (Fig. 1b), shows clear fringes with a planar spacing consistent with well-crystalized tetragonal $CoMn_2O_4$ spinel. The tetragonal distortion is due to a cooperative Jahn-Teller orbital ordering on the octahedral-site high-spin Mn^{3+} ions. EDS gave a Co:Mn ratio 1:1.92, which would correspond to $Co^{2+}[Co^{2+}_{0.03}Mn^{4+}_{0.03}Mn^{3+}_{1.94}]O_4$ for ideal stoichiometry. The powder XRD data of Fig. 2 also show that the CMO particles on graphene obtained in this study have a tetragonal structure corresponding to an atomic site distribution of primarily $Co[Mn_2]O_4$.

Figures 3a–3c show the data for the ORR on CMOG as obtained by the rotating-disk setup. Graphene oxide without any catalyst has an activity for the ORR that is only slightly higher than that of glassy carbon; the defects in the graphene oxide sheets show little activity for the ORR. However, after decoration with CMO nanoparticles, the ORR onset potential is much higher. Where the current reaches −0.1 mA, the CMOG cathode has a potential 220 mV higher than that of the graphene sheets, but it is 90 mV lower than that of a standard cathode of 20 wt % Pt on 80 wt % XC-72. At −1.0 V, the current on the CMOG cathode is about four times higher than that on the graphene oxide sheets. Figure 3b shows the linear scanning voltammograms of the CMOG coated RDE obtained under various rotating speeds from 800 to 2400 rpm. The equation

$$\frac{1}{i} = -\frac{1}{nFAkC^{o}} - \frac{1}{0.62nFAD_{o_2}^{2/3}\upsilon^{-1/6}C^{o}\omega^{1/2}}$$

where i corresponds to the measured current, n is the overall transferred electron number, F is the Faraday constant, C^0 is the saturated concentration of oxygen in 0.1 M KOH solution, A is the geometric area of the electrode, ω is the rotating rate, D_{o2} is the diffusion coefficient of oxygen, υ is the kinetic viscosity of the solution, and k is the rate constant for oxygen reduction, is widely used to analyze the ORR reaction kinetics.[24] The Koutecky-Levich plot is shown in Figure 3c. Based on the average value calculated from different potentials, an overall electron transfer number of 3.9 is obtained, which is quite close to the theoretical value (4.0) for the ORR in alkaline solution.[25]

A catalyst for a rechargeable lithium-air battery needs to have not only ORR activity, but also good OER activity. Figure 3d shows the OER linear scanning voltammogram of a CMOG coated rotating-disk electrode. Compared to the bare glassy carbon electrode, the onset potential is 50 mV lower while the current at 0.5 V is more than five times higher. The calculated current density is 83 A g^{-1} at 0.5 V. Such a considerable OER activity should lead to less polarization while the lithium air battery is charged. It would effectively improve the energy efficiency by decreasing the discharge/charge voltage gap, which is one of the biggest drawbacks of the lithium air battery.

Intensive studies on the lithium air battery have been conducted with carbonate organic electrolytes. However, recent research results indicate such an electrolyte is not suitable for a rechargeable lithium-air battery since the electrolyte can be irreversibly consumed during the discharge process.[26] Nevertheless, the lithium-air primary battery still has potential application because of its theoretical energy density.[27] According to the result of the Bruce group,[26] various lithium organic/inorganic salts are formed with the non-aqueous electrolyte during the first discharge process, most of which stay on the surface of the cathode and lead to failure of a rechargeable Li-air battery. It is important to have an air cathode with a high surface area so that it can accommodate more reaction product. It is well-known that graphene sheets with few layers can reach very high specific surface areas of more than 2000 m^2 g^{-1}, so the CMOG could have a high primary

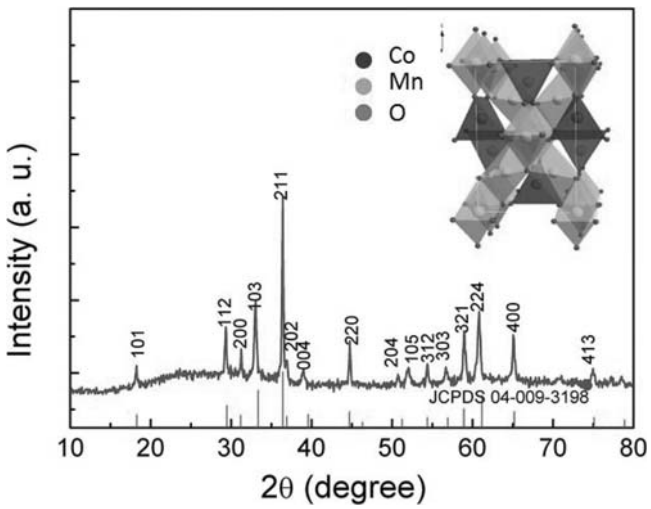

Figure 2. XRD pattern and crystal structure of the CMOG.

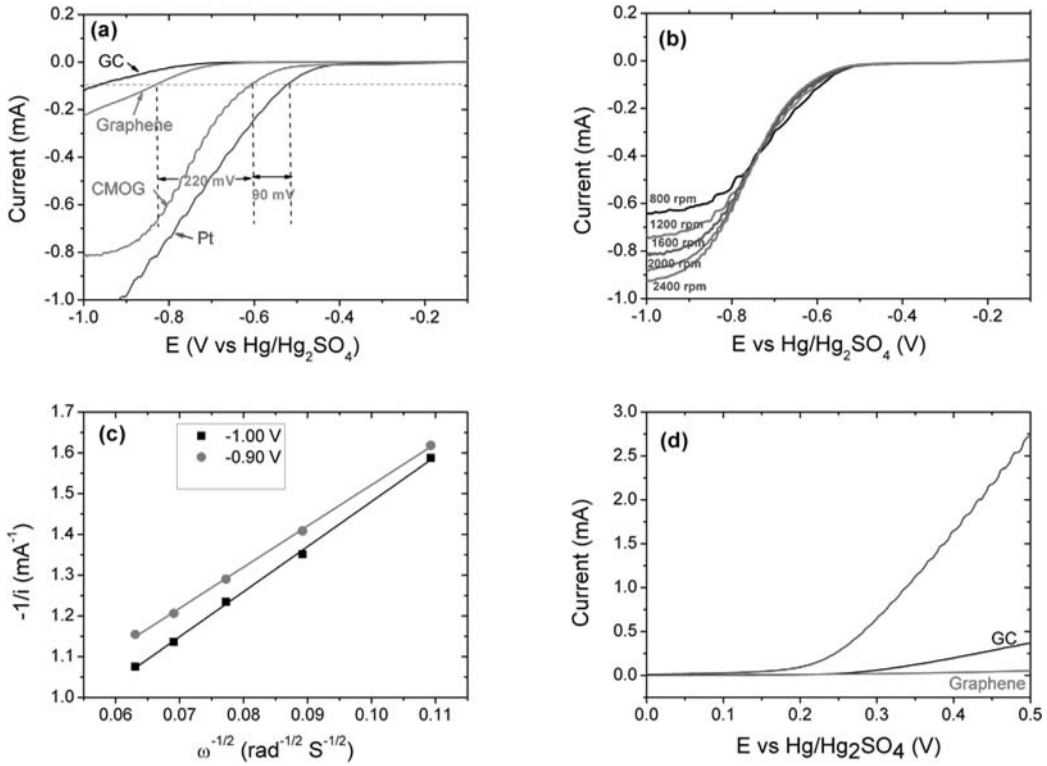

Figure 3. (a) ORR polarization curves of glassy carbon (GC) electrode, 20wt Pt + 80 wt% XC-72 and the CMOG. (b) ORR polarization curves of the CMOG coated electrode under different rotating rates. (c) Koutecky-Levich plot based on ORR polarization curves. (d) OER polarization curves of bare and graphene/CMOG coated-glassy-carbon electrodes.

discharge capacity according to its 2D nanostructure as confirmed by the TEM characterization of Fig. 1. Fig. 4a shows the voltage profile versus capacity calculated from the whole active electrode mass weight. Not surprisingly, a CMOG-based carbon air electrode exhibits as high a discharge capacity as 3000 mA h g^{-1} on the first cycle. Note that the battery is cycled at a constant current density of 0.2 mA cm^{-2}, which is quite different from most reported tests that use a very low current density to reach high capacity. During the following charge process, most of the discharge capacity is not reversible, leading to a rapid capacity fading. From the inset image, we can clearly see that almost no discharge capacity is delivered after the third cycle. The 30 wt % CMOG and 50 wt % AB used in the air cathode is not an optimized ratio; it may be possible to enhance the capacity by optimizing the composition or by changing the AB with another conductive carbon additive.

In contrast to the organic-electrolyte-based lithium-air cells, a cell with an aqueous electrolyte on the cathode side does not have problems with insolvable products from electrochemical reactions. Figure 4b shows the voltage profiles with different current densities. Unlike the carbonate-based lithium-air battery, which generally exhibits more than a 1.0 V gap between charge and discharge, here we find only a 0.3 V gap with a current density of 25 μA cm^{-2}. Such a small difference between charge and discharge originates from a reversible electrochemical reaction

$$4Li + O_2 + 2H_2O \Leftrightarrow 4LiOH$$

If the current density is increased to 2 mA cm^{-2}, a flat voltage curve above 2.5 V is still obtained, indicating a good rate capability of a rechargeable Li-air battery with the cathode in an aqueous alkaline electrolyte. It may also be practical to configure a flow-through battery with a long cycle life by preventing the concentration of LiOH from becoming too high for the solid electrolyte.[28,29]

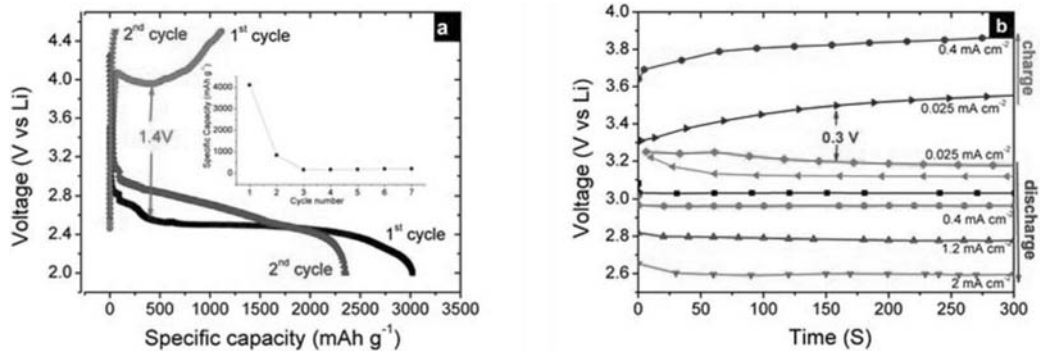

Figure 4. (a) Voltage profiles of first two cycles and cycling performance of non-aqueous electrolyte lithium-air cell charge and discharged at 0.2 mA cm^{-2}. (b) Voltage profiles at different current density of rechargeable lithium-air cell with hybrid electrolyte.

Conclusions

A two-step approach has been achieved to synthesize graphene-supported $CoMn_2O_4$ spinel nanoparticles. Results based on rotating–disk-electrode tests indicate that such a nanostructured catalyst has considerable catalytic activity for both the ORR and the OER. A comparison of a cell having a non-aqueous cathode electrolyte with one having an aqueous cathode electrolyte reveals that graphene-supported $CoMn_2O_4$ spinel nanoparticles can be used as catalyst for lithium-air primary or rechargeable batteries of high energy density.

References

1. K. M. Abraham and Z. Jiang, *J. Electrochem. Soc*., **143**, 1 (1996).
2. T. Kuboki, T. Okuyama, T. Ohsaki, and N. Takami, *J. Power Sources*, **146**, 766 (2005).
3. S. D. Beattie, D. M Manolescu, and S. L. Blair, *J. Electrochem. Soc*., **156**, A44 (2009).
4. Y. C. Lu, Z. C. Xu, H. A. Gasteiger, S. Chen, K. Hamad-Schifferli, and Y. Shao-Horn, *J. Am. Chem. Soc*., **132**, 12170 (2010).
5. A. K. Thapa, K. Saimen, and T. Ishihara, *Electrochem. Solid State Lett*., **13**, A165 (2010).
6. T. Nissinen, Y. Kiros, M. Gasik, and M. Lampinen, *Mater. Res. Bull*., **39**, 1195 (2004).
7. G. Wu, N. Li, D. R. Zhou, K. Mitsuo, and B. Q. Xu, *J. Solid State Chem*., **177**, 3682 (2004).
8. Y. G. Wang and H. S. Zhou, *J. Power Sources*, **195**, 358 (2010).
9. B. A. Lu, D. X. Cao, P. Wang, G. L. Wang, and Y. Y. Gao, *Int. J. Hydrog. Energy*, **36**, 72 (2011).
10. W. J. King and A. C. C. Tseung, *Electrochim. Acta*, **19**, 493 (1974).
11. E. Rios, J. L. Gautier, G. Poillerat, and P. Chartier, *Electrochim. Acta*, **44**, 1491 (1998).
12. F. Y. Cheng, J. A. Shen, B. Peng, Y. D. Pan, Z. L. Tao, and J. Chen, *Nat. Chem*., **3**, 79 (2011).
13. S. M. Paek, E. Yoo, and I. Honma, *Nano Lett*., **9**, 72 (2009).
14. H. L. Wang, L. F. Cui, Y. A. Yang, H. S. Casalongue, J. T. Robinson, Y. Y. Liang, Y. Cui, and H. J. Dai, *J. Am. Chem. Soc*., **132**, 13978 (2010).
15. Y. G. Li, H. L. Wang, L. M. Xie, Y. Y. Liang, G. S. Hong, and H. J. Dai, *J. Am. Chem. Soc*., **133**, 7296 (2011).
16. P. Kundu, C. Nethravathi, P. A. Deshpande, M. Rajamathi, G. Madras, and N. Ravishankar, *Chem. Mat*., **23**, 2772 (2011).
17. Y. Y. Shao, S. Zhang, C. M. Wang, Z. M. Nie, J. Liu, Y. Wang, and Y. H. Lin, *J. Power Sources*, **195**, 4600 (2010).
18. E. Yoo and H. S. Zhou, *ACS Nano*, **5**, 3020 (2011).
19. L. T. Qu, Y. Liu, J. B. Baek, and L. M. Dai, *ACS Nano*, **4**, 1321 (2010).
20. W. S. O. Hummers and R. E. Offeman, *J. Am. Chem. Soc*, **80**,, 1339 (1958).
21. X. J. Zhu, Y. W. Zhu, S. Murali, M. D. Stollers, and R. S. Ruoff, *ACS Nano*, **5**, 3333 (2011).
22. S. Stankovich, R. D. Piner, S. T. Nguyen, and R. S. Ruoff, *Carbon*, **44**, 3342 (2006).
23. Y. H. Lu, J. B. Goodenough, and Y. Kim, *J. Am. Chem. Soc*., **133**, 5756 (2011).
24. F. Y. Cheng, Y. Su, J. Liang, Z. L. Tao, and J. Chen, *Chem. Mat*., **22**, 898 (2010).
25. M. Chatenet, M. Aurousseau, R. Durand, and F. Andolfatto, *J. Electrochem. Soc*., **150**, D47 (2003).
26. S. A. Freunberger, Y. H. Chen, Z. Q. Peng, J. M. Griffin, L. J. Hardwick, F. Barde, P. Novak, and P. G. Bruce, *J. Am. Chem. Soc*., **133**, 8040 (2011).
27. O. Crowther, B. Meyer, M. Morgan, and M. Salomon, *J. Power Sources*, **196**, 1498 (2011).
28. Y. H. Lu and J. B. Goodenough, *Journal of Materials Chemistry*, **21**, 10113 (2011).
29. P. He, Y. G. Wang, and H. S. Zhou, *Electrochem. Commun*., **12**, 1686 (2010).